ACS OMEGA

http://pubs.acs.org/journal/acsodf

Article

Superior ZSM-5@γ-Al_2O_3 Composite Catalyst for Methanol and Ethanol Coconversion to Light Olefins

Liying Zeng, Fei Liu,* Tianxiang Zhao, and Jianxin Cao

Cite This: *ACS Omega* 2021, 6, 19067−19075

Read Online

ACCESS | Metrics & More | Article Recommendations

ABSTRACT: This paper proposes a ZSM-5@γ-Al_2O_3 composite with a core−shell structure for the high-efficiency cocatalytic conversion of a methanol−ethanol system to light olefins. Using ZSM-5 and γ-Al_2O_3 as sole catalysts for comparison, the effects of physical blending, impregnation, and liquid-phase precipitation coating strategies on the catalytic performance and physicochemical properties of the composite catalysts were systematically investigated. The results indicated that the ZSM-5@γ-Al_2O_3 composite catalyst prepared by a liquid-phase precipitation coating exhibited excellent catalytic performance. When the ethanol content was 25 wt % and the reaction occurred at 350 °C, the conversion rates of methanol and ethanol were 96.1 and 99.9%, respectively; the selectivity and yield of light olefins reached 92.3 and 89.9%, respectively. The introduction of ethanol into methanol enhanced the selectivity of light olefins as target products. The interfacial composite phase formed by in situ nucleation growth of pseudoboehmite produced distinct Brønsted−Lewis acid synergistic active centers. It also increased the mesopore/micropore ratio in the composite catalyst.

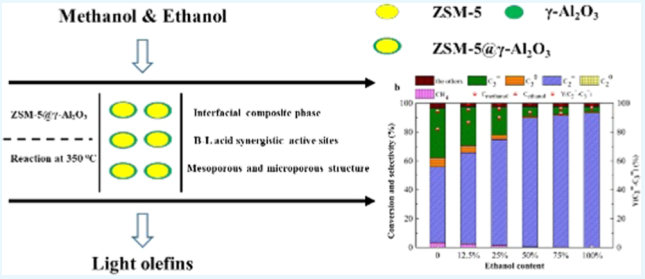

1. INTRODUCTION

In the chemical industry, light olefins (ethylene and propylene) are used to produce a variety of chemicals and polymers,[1−5] such as polyethylene, poly(vinyl chloride), polystyrene,[6,7] polypropylene, acrylic acid, and propylene oxide.[8,9] Currently, the production methods of light olefins mainly include naphtha cracking,[10] propane dehydrogenation,[11] and the catalytic cracking of methanol[12−15] or ethanol.[16,17] Recently, light olefin production strategies employing methanol or ethanol as feedstocks have attracted attention[18,19] because they can enrich the raw materials required for olefin production and also reduce the consumption of petroleum resources.[20,21] Industrial crude methanol obtained from the conversion of coal via synthesis gas usually contains ethanol,[22] making it important to study the direct cocatalysis of ethanol and methanol to olefins. Previous studies have shown that adding ethanol to the methanol-to-light olefin (MTO) process stimulates the formation of hydrocarbons and shortens the induction period of the reaction,[23−26] which helps increase the olefin yield and prolongs the catalyst life.[27] Although the catalytic cracking of methanol and ethanol to olefins have similar dehydration processes, these two compounds have different catalytic activities.

Up to now, a variety of zeolites have been used in methanol conversion reactions.[28−31] When ZSM-5 zeolite is employed as the catalyst, the reaction temperature required for MTO conversion is usually above 400 °C because lower reaction temperatures result in a lower methanol conversion rate and olefin selectivity.[14,32,33] Bakare et al.[34] employed a Mg-ZSM-5-modified catalyst and reached a methanol conversion rate of 100% and a light olefin of 74% at 450 °C. Rostamizadeh et al.[35] used Ni-ZSM-5-modified zeolite as a catalyst and found that the conversion of methanol at 450 °C was 99.9%, and the selectivity of light olefins was 84%. Conversely, ethanol to light olefins (ETO) is more likely to proceed at a lower reaction temperature (about 300 °C) since long-chain hydrocarbon byproducts tend to appear at higher reaction temperatures.[36−38] Zhang et al.[39] used H-ZSM-5 as a catalyst, and the yield of ethylene at 300 °C was around 93.1%. Gayubo et al.[40] employed an AT300-H-ZSM-5-modified catalyst and found that the yield of ethylene reached more than 95% at 280 °C.

Accordingly, when focusing on the production of light olefins using methanol and ethanol as raw materials, it is necessary to first enable the conversion of methanol and ethanol at similar temperatures. From the perspectives of industrial catalysis and practical applications, performing a reaction near the temperature required for the catalytic

Received: May 5, 2021
Accepted: July 5, 2021
Published: July 18, 2021

cracking of ethanol has industrial practicality, but the insufficient activation of the ZSM-5 zeolite toward methanol at low reaction temperatures must be overcome.

Due to its unique MFI topological structure, various and adjustable acid properties, and longer reaction life, ZSM-5 zeolite has been used as an industrial catalyst for this type of reaction. Moreover, its low surface charge density also gives it good hydrothermal stability; however, its microporous structure tends to form coke deposits that can cover the active centers and block pores, thereby limiting the catalytic efficiency.[41−44] To effectively adjust the reaction activity and find a pore structure that is suitable for cocatalyzing the conversion of methanol and ethanol, this paper uses mesoporous γ-Al_2O_3 (with Lewis acid properties)-modified ZSM-5 zeolite to fabricate a composite with a core−shell structure. The expected core−shell structure and properties include more B−L (Brønsted−Lewis) synergistic active centers that promote the dissociation and adsorption of methanol at a lower reaction temperature,[45,46] meso- and micropores that facilitate the diffusion of reactant molecules and slow the generation of coke deposits,[47] and good hydrothermal stability that ensures long-term activity. Therefore, this paper investigates the effects of liquid-phase precipitation coating, impregnation, physical blending, and other compositing methods on the structural properties, catalytic performance, and prevention of coke deposit generation of γ-Al_2O_3/ZSM-5 composite catalysts. The results are used to establish structure−performance relationships of the composite catalysts for methanol−ethanol catalytic conversion.

2. EXPERIMENTAL SECTION

2.1. Catalyst Preparation. *2.1.1. Preparation of γ-Al_2O_3.* γ-Al_2O_3 was prepared by a wet chemical precipitation method. At room temperature, according to a molar ratio between $Al(NO_3)_3{\cdot}9H_2O$ and cetyltrimethylammonium bromide (CTAB) of 2:1, $Al(NO_3)_3{\cdot}9H_2O$ and CTAB were added into deionized water and completely dissolved under stirring to obtain a 0.05 mol·L^{-1} mixed solution. An ammonia solution with a concentration of 1 mol·L^{-1} was pumped at 5 mL·min^{-1} to adjust the pH to 9. The solution was aged in a water bath at 80 °C, and the product was cooled, filtered, and then washed with deionized water and absolute ethanol three times. The washed product was dried at 105 °C for 12 h and calcined at 600 °C for 3 h to obtain mesoporous γ-Al_2O_3.

2.1.2. Preparation of ZSM-5. ZSM-5 zeolite was prepared by hydrothermal synthesis. The molar ratio of raw materials was $TEOS/NaAlO_2/TPAOH/H_2O$ = 30:1:19:8077. Under stirring at room temperature, sodium meta aluminate ($NaAlO_2$) was dissolved in deionized water, and then tetraethylammonium hydroxide (TPAOH) was added after the solution was uniformly stirred. A tetraethyl orthosilicate (TEOS) solution was added dropwise to the solution. After the mixed solution was uniformly stirred and became clear, it was placed in a homogeneous reactor at 180 °C for 48 h to complete the hydrothermal reaction. The product was cooled, filtered, and then washed with deionized water and absolute ethanol 3 times. The washed product was dried at 105 °C for 12 h and calcined at 550 °C for 3 h to prepare ZSM-5 (SiO_2/Al_2O_3 = 60) zeolite.

2.1.3. Preparation of the ZSM-5@γ-Al_2O_3 Composite Catalyst. The composite catalysts with different γ-Al_2O_3 contents were prepared by the liquid-phase precipitation coating method.[45,46] Typically, according to the aforementioned preparation process of γ-Al_2O_3, 3.0 g of the 200-mesh ZSM-5 powder was added to 200 mL of a 0.1 mol·L^{-1} mixed solution of $Al(NO_3)_3{\cdot}9H_2O$ and CTAB. The mixture was stirred uniformly, and a 1 mol·L^{-1} ammonia solution was pumped in at a flow rate of 5 mL·min^{-1} until the solution pH was 9. The solution was aged in a water bath at 80 °C for 3 h. The product was cooled, filtered, and then washed with deionized water and absolute ethanol three times. The washed product was dried at 105 °C for 12 h and calcined at 600 °C for 3 h to obtain a 40% ZSM-5@γ-Al_2O_3-LC composite catalyst.

The composite catalyst was prepared by an impregnation method. According to a γ-Al_2O_3 content of 40%, 3 g of the 200-mesh ZSM-5 powder was added to a 1.0 mol·L^{-1} $Al(NO_3)_3{\cdot}9H_2O$ solution for immersion. A uniform mixture was obtained, and it was allowed to stand for 24 h. The product was dried at 105 °C for 12 h, calcined at 600 °C for 3 h, and the γ-Al_2O_3/ZSM-5-IM composite catalyst was obtained.

The composite catalyst was prepared by a physical blending method. According to a γ-Al_2O_3 content of 40%, 3.0 g of the 200-mesh ZSM-5 powder and 2.0 g of 200-mesh γ-Al_2O_3 were mixed uniformly, and the γ-Al_2O_3/ZSM-5-PB composite catalyst was obtained.

2.2. Catalyst Characterization. The crystalline structure of the catalysts was analyzed and characterized using an X-ray polycrystalline diffractometer (D8-type, Bruker, Germany). The instrument test conditions were as follows: Cu Kα radiation, a scanning rate of 5°·min^{-1}, and a 2θ scanning range of 5−90°. Qualitative and quantitative analyses of the catalyst's elements were performed using a multifunctional X-ray fluorescence spectrometer (Zetium type, PANalytical, the Netherlands). The detection conditions of the instrument were a rhodium target and a power of 3 kW. The specific surface area and pore structure of the catalyst were detected using a surface area and pore analyzer (ASAP2020M, American Micromeritics Company) after the catalyst was degassed for 6 h at 200 °C; the nitrogen adsorption/desorption temperature was −196 °C. The Brunauer−Emmett−Teller (BET) equation, density functional theory (DFT) theory, and *t*-plot method were used to calculate the specific surface area, pore diameter distribution, and pore volume, and the total pores were calculated with P/P_0 = 0.95. The micromorphology of the catalysts was analyzed with a scanning electron microscope (SEM, S-3400N, Hitachi, Japan). The detection conditions of the instrument were an acceleration voltage of 30 kV and a resolution of 3.0 nm. The catalyst microstructure was analyzed with a field emission transmission electron microscope (FEI Titan type 80, Thermo Fisher) under a test voltage of 200 kV. The acid properties of the catalyst surface were characterized by an automatic chemical adsorption analyzer (AutoChem II 2920, Micromeritics Co.). The test procedure was as follows: the temperature was increased from room temperature to 300 °C at a heating rate of 10 °C·min^{-1} and then was decreased to room temperature after holding for 1 h. After 30 min adsorption and 30 min purging, the sample was heated to 700 °C at a rate of 10 °C·min^{-1} for desorption.

Pyridine was used as a probe molecule to detect the type of acids on the catalyst surface with a Fourier transform infrared spectrometer (FTIR, TENSOR27, Bruker, Germany) and high vacuum in situ equipment. The detection procedure was as follows: the sample was placed in a vacuum chamber, heated to 300 °C, and degassed for 2 h. After the vacuum chamber was

https://doi.org/10.1021/acsomega.1c02369
ACS Omega 2021, 6, 19067−19075

cooled to room temperature, pyridine was adsorbed on the surface until saturation was reached. The spectra were collected at 200 and 350 °C. The elemental properties of the catalyst surface were analyzed using a K-Alpha X-ray photoelectron spectrometer (Thermo Fisher Scientific). The test conditions were as follows: Kα X-ray of Al ($h\nu$ = 1486.6 eV) and a power of 150 W. Carbon deposits on the catalyst were analyzed with a thermogravimetric analyzer (TG209, Netzsch, Germany). The test procedure was as follows: approximately 10 mg of the sample was placed in a crucible and heated to 700 °C at a heating rate of 10 °C·min^{-1} and an airflow rate of 20 mL·min^{-1}.

2.3. Evaluation of Catalytic Performance. The catalytic performance was evaluated out on a fixed bed at atmospheric pressure. Two grams of the catalyst was filled into the constant-temperature zone of a fixed-bed stainless steel reaction tube (the upper and lower parts of the tube were filled with quartz wool). After confirming no leaks, methanol and/or ethanol were pumped into the reactor in different ratios under different temperatures. The reaction was carried out with a vaporization temperature of 150 °C, a N_2 flow rate of 100 mL·min^{-1}, and a feed space velocity WHSV = 2 h^{-1}. The reactants and products were detected and analyzed with an online Agilent 7820A gas chromatograph equipped with an FID detector. Using an external standard method, the conversion rates of methanol and ethanol, selectivity, and yield of light olefins were calculated using eqs 1−4. All data were collected after 6 h of reaction.

$$C_{CH_3OH} = \frac{n_{MeOH,in} - n_{MeOH,out}}{n_{MeOH,in}} \times 100\% \quad (1)$$

$$C_{CH_3CH_2OH} = \frac{n_{EtOH,in} - n_{EtOH,out}}{n_{EtOH,in}} \times 100\% \quad (2)$$

$$S_{C_mH_{m+x}} = \frac{m \times n_{C_mH_{m+x}}}{(n_{MeOH,in} - n_{MeOH,out}) + 2(n_{EtOH,in} - n_{EtOH,out})} \times 100\% \quad (3)$$

$$Y_{C_mH_{m+x}} = \frac{m \times n_{C_mH_{m+x}}}{n_{MeOH,in} + 2n_{EtOH,in}} \times 100\% \quad (4)$$

3. RESULTS AND DISCUSSION

3.1. Catalytic Properties. To investigate the effect of different catalysts on the catalytic performance in the MTO at lower reaction temperatures, pure methanol was used as the raw material, and the catalytic performances at 350 °C of γ-Al_2O_3, ZSM-5, ZSM-5@γ-Al_2O_3-LC, γ-Al_2O_3/ZSM-5-IM, and γ-Al_2O_3/ZSM-5-PB were systematically investigated. The catalytic performances of different catalytic systems are shown in Figure 1a. Obviously, the reaction products include CH_4, C_2H_4, C_2H_6, C_3H_6, C_3H_8, and the others. It should be noted that the others include C^{4+} and coke. The carbon atom is conserved during the reaction. At 350 °C, the composite catalyst and the sole catalyst (γ-Al_2O_3 or ZSM-5) have similar methanol conversion rates, all exceeding 90%; however, the olefin selectivity (ethylene and propylene) of sole γ-Al_2O_3 or ZSM-5 catalysts was lower. The olefin yield of the sole γ-Al_2O_3 catalyst was less than 20%, showing the worst catalytic MTO conversion. Compared with the sole catalyst, the catalytic performance of the composite catalyst was significantly enhanced at 350 °C, but different compositing methods

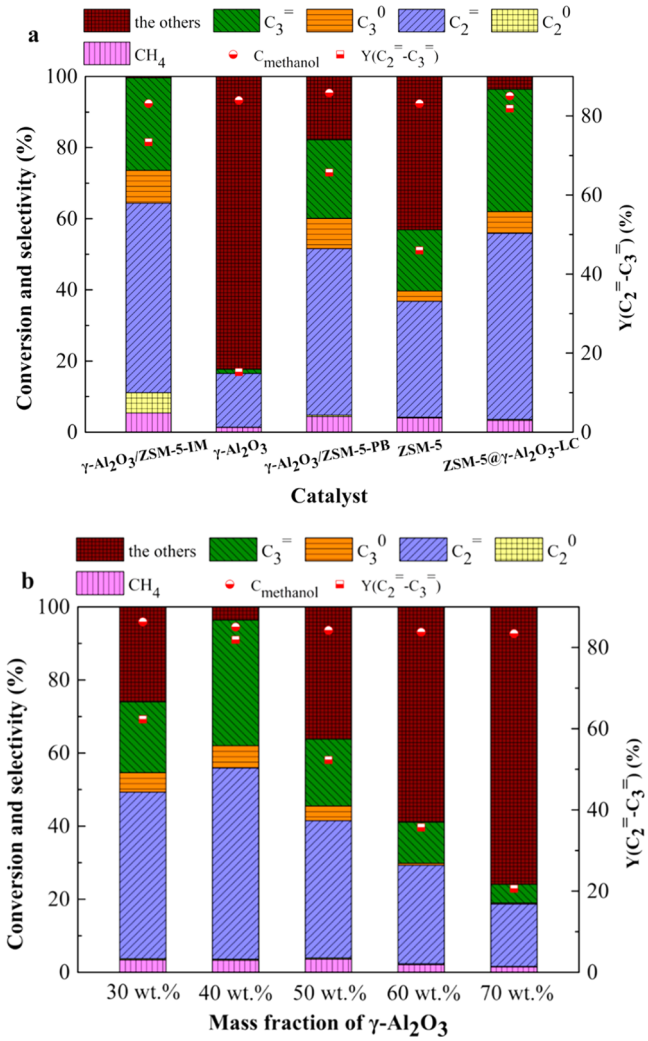

Figure 1. (a) Catalytic performance of various catalysts and (b) catalytic performance of the γ-Al_2O_3@ZSM-5-LC composite with different γ-Al_2O_3 contents. Reaction conditions: WHSV of methanol = 2.0 h^{-1}, 350 °C, and catalyst = 2.0 g. C_2^0 = ethane, $C_2^=$= ethylene, C_3^0 = propane, $C_3^=$= propylene, and the others include C^{4+} byproducts and coke.

significantly impacted the catalytic performance. The ethylene selectivity of γ-Al_2O_3/ZSM-5-PB prepared by physical blending was 46.8%, the propylene selectivity was 22.1%, and the yield of light olefins was 65.7%. For γ-Al_2O_3/ZSM-5-IM prepared by impregnation, the ethylene selectivity was 53.3%, the propylene selectivity was 26.0%, and the light olefin yield was 73.4%. ZSM-5@γ-Al_2O_3-LC prepared by the liquid-phase precipitation coating method showed the best catalytic performance: the ethylene selectivity was 52.3%, the propylene selectivity was 34.4%, and the light olefin yield was 81.9%, which is about 35.9% higher than that of sole ZSM-5.

The mesoporous γ-Al_2O_3 with a Lewis acid center exhibited the lowest catalytic activity toward methanol conversion at 350 °C; however, the catalytic performance of ZSM-5 was significantly higher after compositing with γ-Al_2O_3, possibly because the B (Brønsted) acid and L (Lewis) acid active centers formed on the composite catalyst enhanced the adsorption and dissociation ability of methanol molecules. In addition, compared with the physical blending and impregnation composite methods, the liquid-phase precipitate-coated

https://doi.org/10.1021/acsomega.1c02369
ACS Omega 2021, 6, 19067−19075

samples exhibited the best catalytic performance, possibly because the special interfacial effect of the compositing method forms a novel B−L acid synergistic catalytic mechanism and mesoporous and microporous transport paths. Mesoporous γ-Al_2O_3, with a Lewis acid center, is a hydrophilic material with poor hydrothermal stability at high temperatures. The harsh hydrothermal environment of the MTO reaction easily causes the γ-Al_2O_3 framework to collapse and deactivate. Therefore, when ZSM-5 forms a composite catalyst with γ-Al_2O_3, it is necessary to fully consider the effect of the MTO hydrothermal environment on the structural stability of the composite catalyst.

The γ-Al_2O_3 content also significantly affected the catalytic performance of the composite catalyst. When the γ-Al_2O_3 content was 40%, ZSM-5@γ-Al_2O_3-LC showed the best catalytic performance (Figure 1b) and also had better hydrothermal stability and better resistance to carbon deposition and deactivation. After the reaction for 50 h, the crystal form and crystallinity of the composite catalyst did not change (Figure 2). In addition, the spent ZSM-5 zeolite had

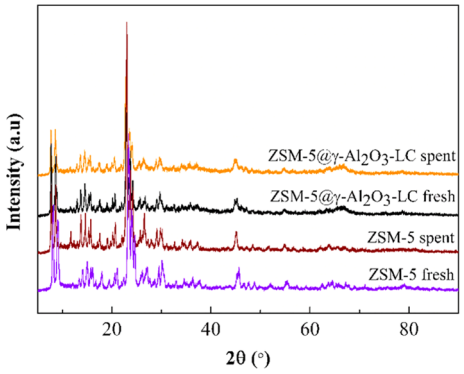

Figure 2. X-ray diffraction (XRD) patterns of the fresh and spent ZSM-5@γ-Al_2O_3-LC and ZSM-5.

the most carbon deposit due to its micropore structure, but the spent composite catalysts displayed a small amount of coke deposit (Figure 3), suggesting that the formation of mesopores in the composite catalyst helped alleviate the formation of coke deposits.

The MTO catalytic performance of the ZSM-5@γ-Al_2O_3-LC composite catalyst within a reaction temperature range of 300−450 °C was investigated, and the results are shown in Figure 4a. As the reaction temperature increased, the methanol

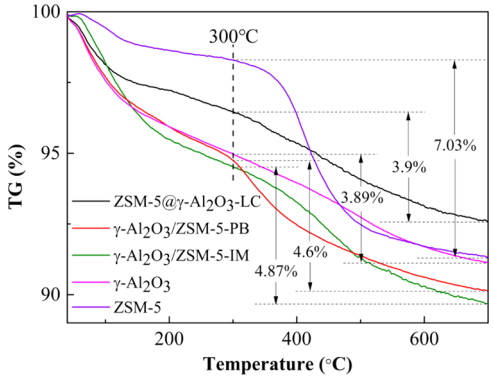

Figure 3. TG curves of various spent catalysts.

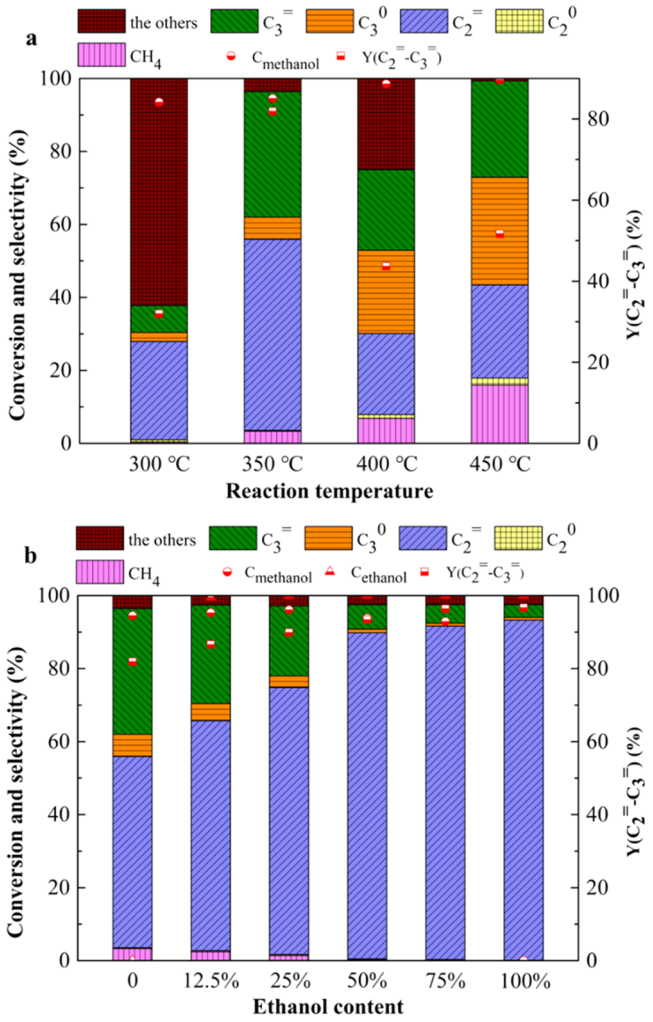

Figure 4. (a) Dependence of catalytic performance over the ZSM-5@γ-Al_2O_3-LC composite on various reaction temperatures and (b) dependence of catalytic performance over the ZSM-5@γ-Al_2O_3-LC composite on various ethanol contents. Reaction conditions: WHSV of alcohol = 2.0 h^{-1}, 350 °C, and catalyst = 2.0 g. C_2^0 = ethane, $C_2^=$= ethylene, C_3^0 = propane, $C_3^=$= propylene, and the others include C^{4+} byproducts and coke.

conversion rate increased slowly, but the olefin yield exhibits a volcano shape as the reaction temperature increased and reached a maximum at 350 °C. A higher reaction temperature enhanced the activation and dissociation of methanol molecules induced by the composite catalyst, causing the methanol conversion to increase with the reaction temperature; however, a reaction temperature that is excessively high or low will decrease the ethylene and propylene selectivities to varying degrees. The reduction may occur because low reaction temperatures tend to produce ethers, while high reaction temperatures are more likely to form long-chain hydrocarbon products. The liquid-phase precipitation coating method was used to modify the microporous ZSM-5 zeolite with B acid properties using mesoporous γ-Al_2O_3 with the characteristics of L acid. This strategy enhanced the activation, dissociation, and conversion capability of the composite catalyst toward methanol molecules at 350 °C. This finding demonstrates the feasibility of methanol−ethanol cocatalytic conversion to olefins at lower reaction temperatures.

https://doi.org/10.1021/acsomega.1c02369
ACS Omega 2021, 6, 19067−19075

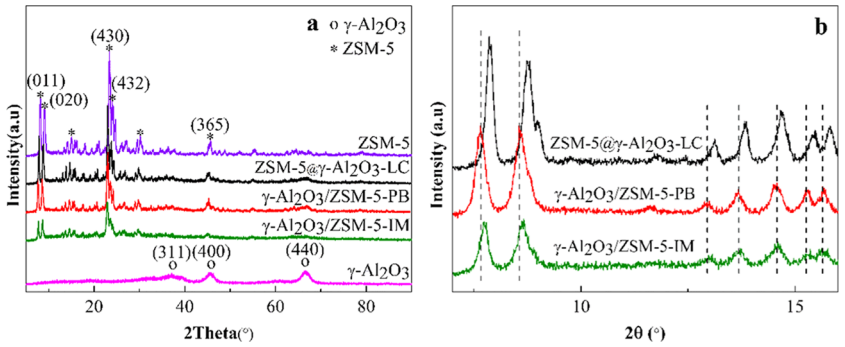

Figure 5. (a) XRD patterns of various catalysts and (b) enlarged view of ZSM-5@γ-Al_2O_3-LC, γ-Al_2O_3/ZSM-5-PB, and γ-Al_2O_3/ZSM-5-IM (2θ = 7−16°).

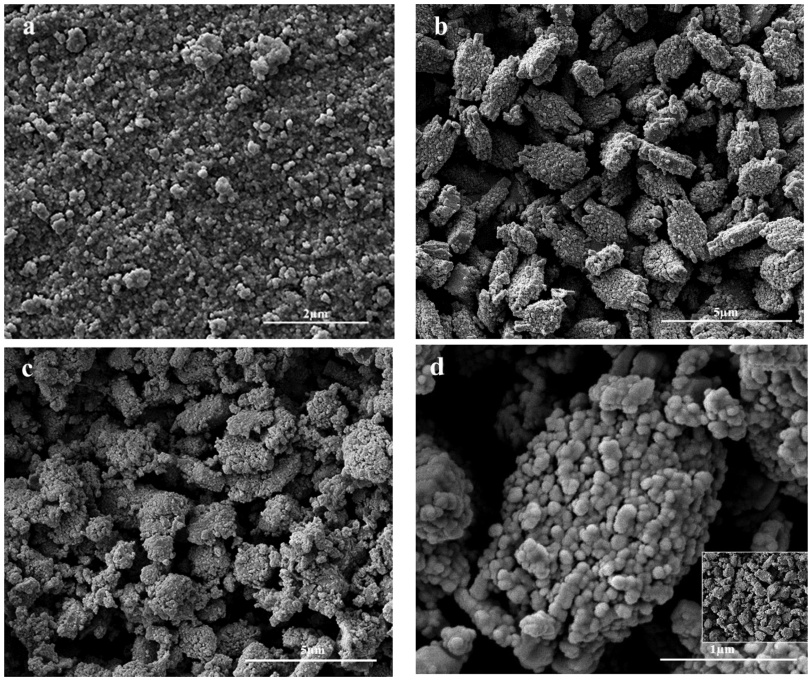

Figure 6. SEM images of various samples: (a) γ-Al_2O_3, (b) ZSM-5, (c) γ-Al_2O_3/ZSM-5-PB, and (d) ZSM-5@γ-Al_2O_3-LC.

The catalytic performance of ZSM-5@γ-Al_2O_3-LC during methanol−ethanol conversion with different ethanol content is shown in Figure 4b. At 350 °C, ZSM-5@γ-Al_2O_3-LC displayed better catalytic performance for the ETO process, with a 100% ethanol conversion rate and 96.7% light olefin selectivity. Interestingly, during MTO, the conversion rate of ethanol was always near 100%, and as the content of ethanol increased, the light olefin selectivity increased from 81.9 to 96.7%. However, the conversion rate of methanol first increased and then slightly decreased but was always higher than 90%. When the ethanol content was 25%, the conversion rates of methanol and ethanol were 96.1 and 99.9%, respectively; the selectivity and yield of light olefins reached 92.3 and 89.9%, respectively.

During the methanol−ethanol cocatalytic conversion to olefins, the dehydration of methanol to olefins is exothermic, while the dehydration of ethanol to olefins is endothermic. The simultaneous progress of the two reactions maintained the endothermic/exothermic equilibrium of the system. Thermodynamically, ethanol dehydrates easier than methanol, and when methanol and ethanol coreact, the two alcohol molecules compete for acidic sites. Furthermore, ethanol tends to be more predominant than methanol because it can preferentially occupy acid sites on the catalyst surface. As the content of ethanol in the MTO process increases, the product distribution is more similar to that obtained using the ETO process. Although the methanol conversion rate slightly decreased due to competitive adsorption, the olefin yield increased in the methanol−ethanol cocatalytic process. It can be seen that ZSM-5@γ-Al_2O_3-LC with 40% γ-Al_2O_3 prepared by the liquid-phase precipitation coating method was favorable for the catalytic cracking of methanol, and also helped inhibit the formation of byproducts during ETO conversion. Therefore, the composite catalyst efficiently converted methanol and ethanol to light olefins at 350 °C.

3.2. Structure and Properties of Catalysts. To reveal the structure−performance relationship of the catalyst, γ-Al_2O_3 and ZSM-5 catalysts were used to comparatively study the physicochemical properties of different composite catalysts. The XRD patterns of the different catalysts are shown in Figure 5. The XRD patterns of γ-Al_2O_3 or ZSM-5 catalysts are in complete agreement with those shown in standard cards (PDF No. 10-0425 and PDF No. 44-0003, respectively), indicating their high purity. The intensity of the diffraction peaks of ZSM-5 and γ-Al_2O_3 in the γ-Al_2O_3/ZSM-5-IM sample

https://doi.org/10.1021/acsomega.1c02369
ACS Omega 2021, 6, 19067−19075

prepared by the impregnation method were both weakened. The diffraction peaks of γ-Al_2O_3 were more pronounced, and some of the diffraction peaks of ZSM-5 shifted to slightly larger angles (Figure 5b). The results indicate that the γ-Al_2O_3 component loaded onto the pores of ZSM-5 zeolite was dispersed, exhibiting a certain interfacial interaction. Both the physically blended sample and the liquid-phase coated sample exhibited characteristic diffraction peaks of ZSM-5 (PDF No. 44-0003) and γ-Al_2O_3 (PDF No. 10-0425), indicating that both crystal phases existed in γ-Al_2O_3/ZSM-5-PB and ZSM-5@γ-Al_2O_3-LC composite samples. However, compared with γ-Al_2O_3/ZSM-5-PB, the 2θ angle corresponding to a part of the ZSM-5 diffraction peaks of ZSM-5@γ-Al_2O_3-LC significantly shifted to larger angles (Figure 5b), indicating a reduction in the spacing between crystal planes.

During liquid-phase coating preparation, the ZSM-5 solid powder was put into a synthesis reaction system containing γ-Al_2O_3. After the addition of an alkaline precipitant, the pseudoboehmite precursor formed by the precipitation reaction adhered to the surface of ZSM-5 grains and then underwent in situ nucleation and growth. The formation of a special composite interfacial phase thereby partly reduced the crystal plane spacing of ZSM-5. Different compositing methods significantly impacted the structures of the composite phases, which was also verified by the SEM and high-resolution TEM (HRTEM) analysis of different catalysts. The SEM result shows that γ-Al_2O_3 consists of typically nearly spherical nanoparticles (Figure 6a), while the ZSM-5 zeolite with Si/Al=60 is formed with micron-sized irregular blocks with rough surfaces (Figure 6b). The morphology of γ-Al_2O_3/ZSM-5-PB was only a simple physical mixture of two phases (Figure 6c), without any special chemical interfaces. In ZSM-5@γ-Al_2O_3-LC, the spherical γ-Al_2O_3 nanoparticles were attached to the surface of the irregular ZSM-5 blocks (Figure 6d).

To further reveal the special composite phase structure of the ZSM-5@γ-Al_2O_3-LC catalyst, the liquid-phase-coated sample was analyzed and characterized by HRTEM (Figure 7). The crystal lattice spacings of grains on the surface of ZSM-5 were 0.139 and 0.198 nm, which correspond to the (440) and (400) crystal planes of γ-Al_2O_3. These results confirm that

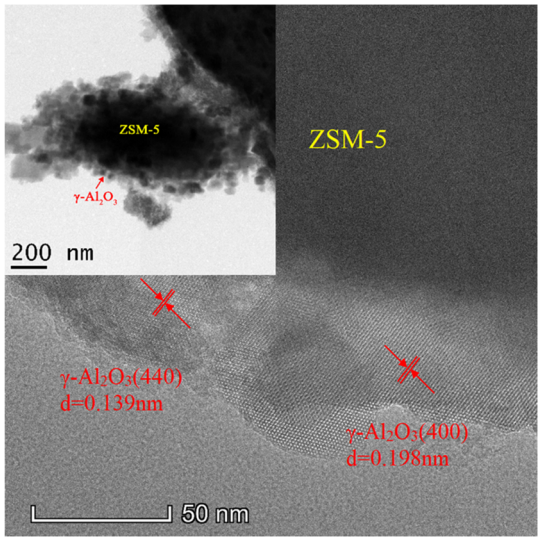

Figure 7. HRTEM images of the composite sample ZSM-5@γ-Al_2O_3-LC.

the micron-sized ZSM-5 grains were covered by many nearly spherical γ-Al_2O_3 nanograins, and the two phases showed a higher affinity, indicating that a composite interface formed between the two phases, which gave rise to novel physicochemical properties.

The N_2 adsorption−desorption isotherms and pore structure parameters of different catalysts are shown in Figure 8 and

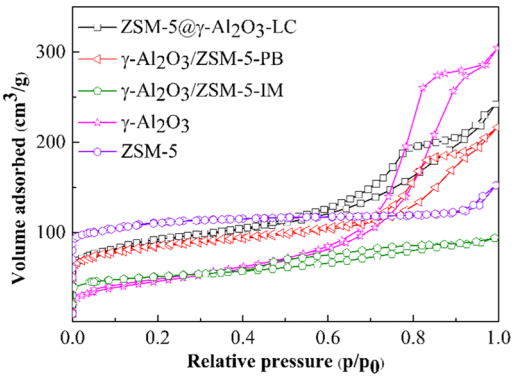

Figure 8. N_2 adsorption/desorption isotherms of various catalysts.

Table 1. Specific Surface Area, Pore Volume, and Average Pore Diameter Data of Various Catalysts

	BET surface area ($m^2 \cdot g^{-1}$)			pore volume ($cm^3 \cdot g^{-1}$)			
samples	S_{BET}	S_{mic}	S_{mes}	V_t	V_{mic}	V_{mes}	pore diameter (nm) D
ZSM-5@γ-Al_2O_3-LC	296	158	138	0.33	0.08	0.25	4.4
γ-Al_2O_3/ZSM-5-PB	267	172	95	0.30	0.09	0.21	4.4
γ-Al_2O_3/ZSM-5-IM	164	91	73	0.15	0.05	0.10	3.5
γ-Al_2O_3	169	5	164	0.45		0.45	9.8
ZSM-5	338	311	27	0.20	0.16	0.04	2.3

Table 1. γ-Al_2O_3 mainly exhibited typical characteristics of a mesoporous structure, while ZSM-5 zeolite was a typical microporous material. The composite catalysts all exhibited characteristics of both mesoporous and microporous structures, and the specific surface area of micropores was higher than that of mesopores because the content of the mesoporous γ-Al_2O_3 phase was only 40%. Compared with γ-Al_2O_3/ZSM-5-PB, the decline of both the micropore and mesopore volumes of γ-Al_2O_3/ZSM-5-IM may be related to the blocking of micropores of ZSM-5 and/or the breaking of the framework of ZSM-5 during the wet impregnation process. Interestingly, the mesopore/micropore ratio in ZSM-5@γ-Al_2O_3-LC was significantly promoted in comparison with γ-Al_2O_3/ZSM-5-PB. During the preparation of a liquid-phase precipitation coating, the formation of special composite interfacial phases enhanced the mesopore structure characteristics of the composite catalyst to a certain extent. During MTO and ETO conversion, although the shape-selective function of the microporous structure is favorable for the production of small olefins such as ethylene and propylene, it also aggravates the conversion of intermediates into coke deposits, which block micropores and

https://doi.org/10.1021/acsomega.1c02369
ACS Omega 2021, 6, 19067−19075

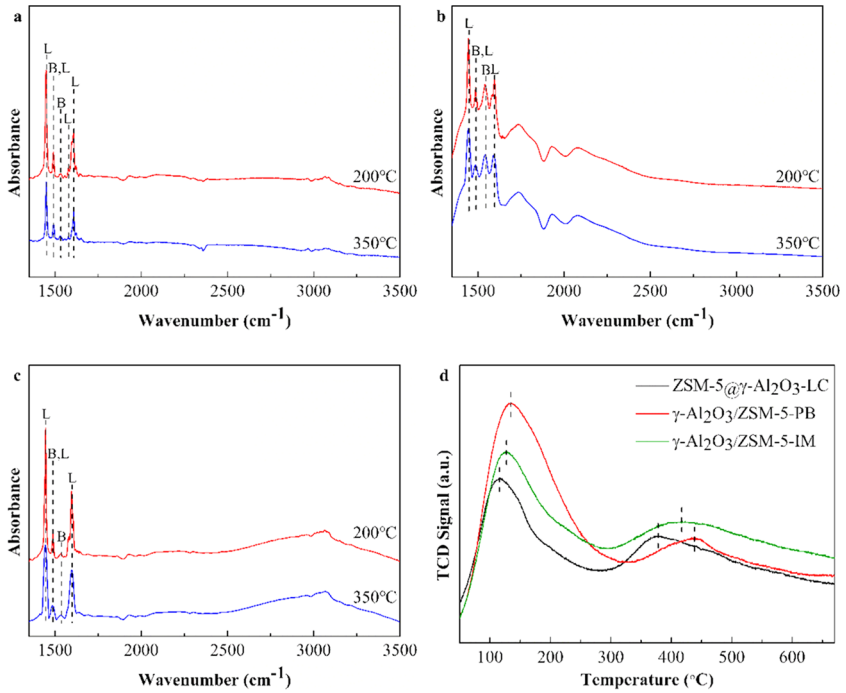

Figure 9. (a) Py-FTIR spectra of ZSM-5@γ-Al_2O_3-LC; (b) Py-FTIR spectra of γ-Al_2O_3/ZSM-5-PB; (c) Py-FTIR spectra of γ-Al_2O_3/ZSM-5-IM; and (d) NH_3-TPD profiles of various composite catalysts.

quickly deactivate the catalyst. The formation of mesoporous and microporous systems promoted molecular diffusion and alleviated the formation of carbon deposits.

The formation of an interfacial composite phase also provided novel Brønsted (1490 and 1535 cm^{-1})−Lewis acid (1450, 1490, 1575, and 1610 cm^{-1}) synergistic active centers (Figure 9a and Table 2) in the composite catalyst. Additionally, to a certain extent, the introduction of L acids and the formation of the interfacial phase decreased the total acid strength (Figure 9d). These modifications not only helped enhance the catalytic activity of ZSM-5 during the MTO reaction at lower reaction temperatures but also inhibited the formation of byproducts in the ETO reaction and alleviated the formation of carbon deposits.

Table 2. L Acid and B Acid Amounts of ZSM-5@γ-Al_2O_3-LC

temperature (°C)	B acid amount (μmol/g)	L acid amount (μmol/g)	total acid (μmol/g)
200	3.15	66.36	69.51
350	1.73	35.19	36.92

Although γ-Al_2O_3/ZSM-5-PB and γ-Al_2O_3/ZSM-5-IM composite catalysts also exhibited meso/microporous systems and B−L acid active centers, γ-Al_2O_3/ZSM-5-PB was only physically mixed, and no interfacial phase was formed, so it has a weaker synergistic mechanism and a slightly higher catalytic performance. In contrast, γ-Al_2O_3/ZSM-5-IM displayed two-phase interfacial interactions due to the loading effect, but the impregnation method was more likely to substantially decrease the specific surface area and pore volume of the mesopores and micropores, which inhibited its catalytic performance.

4. CONCLUSIONS

The ZSM-5@γ-Al_2O_3-LC composite catalyst prepared by the liquid-phase precipitation coating method enhanced the catalytic performance for methanol dehydration in the MTO reaction at 350 °C, reaching a conversion rate of 94.5% and a light olefin selectivity of 86.7%. The composite catalyst also exhibited excellent catalytic performance in the cocatalytic system for a methanol−ethanol mixture. At 350 °C, when the ethanol content was 25 wt % in the alcohol mixture, the conversion rate of methanol was 96.1%, the conversion rate of ethanol was 99.9%, and the selectivity and yield of olefins reached 92.3 and 89.9%, respectively. The incorporation of ethanol in the cocatalytic system for methanol−ethanol further enhanced the selectivity and yield of the light olefins.

In the composites prepared by the liquid-phase precipitation coating, the interfacial phase formed by the in situ nucleation growth of pseudoboehmite enriched the types of acid centers and weakened their strength. This also increased the mesopore/micropore ratio in the composite catalyst. These novel changes in physicochemical properties are the crucial factors for improving the efficient cocatalytic conversion of methanol and ethanol to light olefins.

AUTHOR INFORMATION

Corresponding Author

Fei Liu − *School of Chemistry and Chemical Engineering, Guizhou University, Guiyang, Guizhou 550025, P. R. China; Key Laboratory of Green Chemical and Clean Energy Technology and Engineering Research Center of Efficient Utilization for Industrial Waste, Guizhou University, Guiyang, Guizhou 550025, P. R. China;* orcid.org/0000-0003-3775-0035; Email: ce.feiliu@gzu.edu.cn

Authors

Liying Zeng − *School of Chemistry and Chemical Engineering, Guizhou University, Guiyang, Guizhou 550025, P. R. China;*

https://doi.org/10.1021/acsomega.1c02369
ACS Omega 2021, 6, 19067−19075

Key Laboratory of Green Chemical and Clean Energy Technology and Engineering Research Center of Efficient Utilization for Industrial Waste, Guizhou University, Guiyang, Guizhou 550025, P. R. China; orcid.org/0000-0001-6288-1497

Tianxiang Zhao − *School of Chemistry and Chemical Engineering, Guizhou University, Guiyang, Guizhou 550025, P. R. China; Key Laboratory of Green Chemical and Clean Energy Technology and Engineering Research Center of Efficient Utilization for Industrial Waste, Guizhou University, Guiyang, Guizhou 550025, P. R. China;* orcid.org/0000-0001-8197-2423

Jianxin Cao − *School of Chemistry and Chemical Engineering, Guizhou University, Guiyang, Guizhou 550025, P. R. China; Key Laboratory of Green Chemical and Clean Energy Technology and Engineering Research Center of Efficient Utilization for Industrial Waste, Guizhou University, Guiyang, Guizhou 550025, P. R. China*

Complete contact information is available at: https://pubs.acs.org/10.1021/acsomega.1c02369

Notes

The authors declare no competing financial interest.

■ ACKNOWLEDGMENTS

This work was supported by Scientific and Technological Innovation Talents Team Project of Guizhou Province (No. 20185607), One Hundred Person Project of Guizhou Province (No. 20165655), Innovation Group Project of Education Department in Guizhou Province (No. 2021010), Excellent Young Scientific and Technological Talent Program of Guizhou Province (No. 20195645), and Zunyi City Innovative Talent Team Project (No. 20195645).

■ REFERENCES

(1) Yang, M.; You, F. Comparative Techno-economic and Environmental Analysis of Ethylene and Propylene Manufacturing from Wet Shale Gas and Naphtha. *Ind. Eng. Chem. Res.* **2017**, *56*, 4038−4051.

(2) Masih, D.; Rohani, S.; Kondo, J. N.; Tatsumi, T. Catalytic dehydration of ethanol-to-ethylene over Rho zeolite under mild reaction conditions. *Microporous Mesoporous Mater.* **2019**, *282*, 91−99.

(3) Liu, Z.; Ren, S.; Yu, X.; Chen, X.; Wang, G.; Wu, X.; Yu, G.; Qiu, M.; Yang, C.; Sun, Y. Melting-assisted solvent-free synthesis of hierarchical SAPO-34 with enhanced methanol to olefins (MTO) performance. *Catal Sci Technol.* **2018**, *8*, 423−427.

(4) Jiang, X.; Su, X. F.; Bai, X. F.; Li, Y. Z.; Yang, L.; Zhang, K.; Zhang, Y.; Liu, Y.; Wu, W. Conversion of methanol to light olefins over nanosized [Fe, Al]ZSM-5 zeolites: Influence of Fe incorporated into the framework on the acidity and catalytic performance. *Microporous Mesoporous Mater.* **2018**, *263*, 243−250.

(5) Ali, M. A.; Al-Baghli, N. A.; Nisar, M.; Malaibari, Z. O.; Abutaleb, A.; Ahmed, S. J. E. Selective Production of Propylene from Methanol over Monolith Supported Modified ZSM-5 Catalysts. *Energy Fuels* **2019**, *33*, 1458−1466.

(6) Khamkeaw, A.; Phanthang, L.; Jongsomjit, B.; Phisalaphong, M. Activated carbon derived from bacterial cellulose and its use as catalyst support for ethanol conversion to ethylene. *Catal. Commun.* **2019**, *129*, No. 105750.

(7) Zhang, M.; Yu, Y. Dehydration of Ethanol to Ethylene. *Ind. Eng. Chem. Res.* **2013**, *52*, 9505−9514.

(8) Xue, F.; Miao, C.; Yue, Y.; Hua, W.; Gao, Z. Sc_2O_3-promoted composite of In_2O_3 and Beta zeolite for direct conversion of bio-ethanol to propylene. *Fuel Process Technol.* **2019**, *186*, 110−115.

(9) Khanmohammadi, M.; Amani, S.; Garmarudi, A. B.; Niaei, A. Methanol-to-propylene process: Perspective of the most important catalysts and their behavior. *Chin. J. Catal.* **2016**, *37*, 325−339.

(10) Hashemi, F.; Taghizadeh, M.; Rami, M. D. Polyoxometalate modified SAPO-34: A highly stable and selective catalyst for methanol conversion to light olefins. *Microporous Mesoporous Mater.* **2020**, *295*, No. 109970.

(11) Nawaz, Z. Light alkane dehydrogenation to light olefin technologies: a comprehensive review. *Rev Chem Eng.* **2015**, *31*, 413−436.

(12) Rostamizadeh, M.; Taeb, A. Highly selective Me-ZSM-5 catalyst for methanol to propylene (MTP). *J. Ind. Eng. Chem.* **2015**, *27*, 297−306.

(13) Ahmadpour, J.; Taghizadeh, M. Catalytic conversion of methanol to propylene over high-silica mesoporous ZSM-5 zeolites prepared by different combinations of mesogenous templates. *J. Nat. Gas Sci. Eng.* **2015**, *23*, 184−194.

(14) Feng, R.; Yan, X.; Hu, X.; Zhang, Y.; Wu, J.; Yan, Z. Phosphorus-modified b-axis oriented hierarchical ZSM-5 zeolites for enhancing catalytic performance in a methanol to propylene reaction. *Appl. Catal., A* **2020**, *594*, No. 117464.

(15) Rodríguez-Vallej, D. F.; Guillen-Gosalbez, G.; Chachuat, B. What Is the True Cost of Producing Propylene from Methanol? The Role of Externalities. *ACS Sustainable Chem. Eng.* **2020**, *8*, 3072−3081.

(16) Garbarino, G.; Raam, P. P. V.; Paola, R.; Elisabetta, F.; Guido, B. Ethanol and diethyl ether catalytic conversion over commercial alumina and lanthanum-doped alumina: Reaction paths, catalyst structure and coking. *Appl. Catal., B* **2018**, *236*, 490−500.

(17) Wang, F.; Xia, W.; Mu, X.; Chen, K.; Si, H.; Li, Z. A combined experimental and theoretical study on ethanol conversion to propylene over Y/ZrO_2 catalyst. *Appl. Surf. Sci.* **2018**, *439*, 405−412.

(18) Hu, X.; Yuan, L.; Cheng, S.; Luo, J.; Sun, H.; Li, S.; Li, L.; Wang, C. GeAPSO-34 molecular sieves: Synthesis, characterization and methanol-to-olefins performance. *Catal. Commun.* **2019**, *123*, 38−43.

(19) Clemente, M. C. H.; Martins, G. A. V.; Freitas, E.; Dias, J. A.; Dias, S. C. L. Ethylene production via catalytic ethanol dehydration by 12-tungstophosphoric. *Fuel* **2019**, *239*, 491−501.

(20) Bokade, V. V.; Yadav, G. D. Heteropolyacid supported on montmorillonite catalyst for dehydration of dilute bio-ethanol. *Appl. Clay Sci.* **2011**, *53*, 263−271.

(21) Chen, Y.; Wu, Y.; Tao, L.; Dai, B.; Yang, M.; Chen, Z.; Zhu, X. Dehydration reaction of bio-ethanol to ethylene over modified SAPO catalysts. *J. Ind. Eng. Chem.* **2010**, *16*, 717−722.

(22) Jiang, L.; Li, C.; Xu, M.; Xing, A.; Feng, R.; Wu, J. Investigation on and industrial application of degrading of methanol feed in methanol to propylene process. *Chin. J. Chem. Eng.* **2018**, *26*, 2102−2111.

(23) Song, W.; Marcus, D. M.; Fu, H.; Ehresmann, J. O.; Haw, J. F. An oft-studied reaction that may never have been: Direct catalytic conversion of methanol or dimethyl ether to hydrocarbons on the solid acids HZSM-5 or HSAPO-34. *J. Am. Chem. Soc.* **2002**, *124*, 3844−3845.

(24) Mole, T.; Whiteside, J. A.; Seddon, D. Aromatic co-catalysis of methanol conversion over zeolite catalysts. *J. Catal.* **1983**, *82*, 261−266.

(25) Chen, J. Q.; Bozzano, A.; Glover, B.; Fuglerud, T.; Kvisle, S. Recent advancements in ethylene and propylene production using the UOP/Hydro MTO process. *Catal. Today* **2005**, *106*, 103−107.

(26) Vogt, C.; Weckhuysen, B. M.; Ruizmartínez, J. Effect of Feedstock and Catalyst Impurities on the Methanol-to-Olefin Reaction over H-SAPO-34. *ChemCatChem.* **2017**, *9*, 183−194.

(27) Feng, R.; Yan, X.; Hu, X.; Zhang, Y.; Yan, Z. The effect of co-feeding ethanol on a methanol to propylene (MTP) reaction over a commercial MTP catalyst. *Appl. Catal., A* **2020**, *592*, No. 117429.

(28) Ding, J.; Zhang, Z.; Meng, C.; Zhao, G.; Liu, Y.; Lu, Y. From nano-to macro-engineering of ZSM-11 onto thin-felt stainless-steel-

fiber: Steam-assisted crystallization synthesis and methanol-to-propylene performance. *Catal Today* **2020**, *347*, 10−17.
(29) Wang, S.; Wei, Z.; Chen, Y.; Qin, Z.; Ma, H.; Dong, M.; Fan, W.; Wang, J. Methanol to Olefins over H-MCM-22 Zeolite: Theoretical Study on the Catalytic Roles of Various Pores. *ACS Catal.* **2015**, *5*, 1131−1144.
(30) Sun, Q.; Wang, N.; Guo, G.; Yu, J. Ultrafast synthesis of nano-sized zeolite SAPO-34 with excellent MTO catalytic performance. *Chem. Commun.* **2015**, *51*, 16397−16400.
(31) Gao, B.; Miao, Y.; Qiao, Y.; Li, J.; Xiao, X.; Wu, P.; Wei, Y.; Xu, S.; Peng, T.; Liu, Z. A low-temperature approach to synthesize low-silica SAPO-34 nanocrystals and their application in the methanol-to-olefins (MTO) reaction. *Catal. Sci. Technol.* **2016**, *6*, 7569−7578.
(32) Khaledi, K.; Haghighi, M.; Sadeghpour, P. On the catalytic properties and performance of core-shell ZSM-5@MnO nanocatalyst used in conversion of methanol to light olefins. *Microporous Mesoporous Mater.* **2017**, *246*, 51−61.
(33) Losch, P.; Pinar, A. B.; Willinger, M. G.; Soukup, K.; Louis, B.; et al. H-ZSM-5 zeolite model crystals: Structure-diffusion-activity relationship in methanol-to-olefins catalysis. *J. Catal.* **2017**, *345*, 11−23.
(34) Bakare, I. A.; Muraza, O.; Yamani, Z. H.; Yoshioka, M.; Yokoi, T. Conversion of methanol to olefins over Al-rich ZSM-5 modified with alkaline earth metal oxides. *Catal. Sci. Technol.* **2016**, *6*, 7852−7859.
(35) Rostamizadeh, M.; Yaripour, F.; Hazrati, H. Ni-doped high silica HZSM-5 zeolite (Si/Al=200) nanocatalyst for the selective production of olefins from methanol. *J. Anal. Appl. Pyrolysis* **2018**, *132*, 1−10.
(36) Lu, J.; Liu, Y.; Li, N. Fe-modified HZSM-5 catalysts for ethanol conversion into light olefins. *J. Nat. Gas Chem.* **2011**, *20*, 423−427.
(37) Van der Borght, K.; Galvita, V. V.; Marin, G. B. Ethanol to higher hydrocarbons over Ni, Ga, Fe-modified ZSM-5: Effect of metal content. *Appl. Catal., A* **2015**, *492*, 117−126.
(38) Phung, T. K.; Busca, G. Diethyl ether cracking and ethanol dehydration: Acid catalysis and reaction paths. *Chem. Eng. J.* **2015**, *272*, 92−101.
(39) Zhang, X.; Wang, R.; Yang, X.; Zhang, F. Comparison of four catalysts in the catalytic dehydration of ethanol to ethylene. *Microporous Mesoporous Mater.* **2008**, *116*, 210−215.
(40) Gayubo, A. G.; Alonso, A.; Valle, B.; Aguayo, A. T.; Bilbao, J. Selective production of olefins from bioethanol on HZSM-5 zeolite catalysts treated with NaOH. *Appl. Catal., B* **2010**, *97*, 299−306.
(41) Sousa, Z. S. B.; Cláudia, O. V.; Cristiane, A. H.; Victor, T. S. Ethanol conversion into olefins and aromatics over HZSM-5 zeolite: Influence of reaction conditions and surface reaction studies. *J. Mol. Catal., A* **2016**, *422*, 266−274.
(42) Kondo, J. N.; Ito, K.; Yoda, E.; Wakabayashi, F.; Domen, K. An Ethoxy Intermediate in Ethanol Dehydration on Brønsted Acid Sites in Zeolite. *J. Phys. Chem. B* **2005**, *109*, 10969−10972.
(43) Abu-Dahrieh, J.; Rooney, D.; Goguet, A.; Saih, Y. Activity and deactivation studies for direct dimethyl ether synthesis using CuO-ZnO-Al_2O_3 with NH_4ZSM-5, HZSM-5 or γ-Al_2O_3. *Chem. Eng. J.* **2012**, *203*, 201−211.
(44) Volkov, V. V.; Novitskii, E. G.; Dibrov, G. A.; Samokhin, P. V.; Kipnis, M. A.; Yaroslavtsev, A. B. Catalytic conversion of methanol to dimethyl ether on polymer/ceramic composite membranes. *Catal. Today* **2012**, *193*, 31−36.
(45) Liu, P.; Cao, J.; Xu, Z.; Yang, C.; Wang, X.; Liu, F. Thiolation of methanol with H_2S using core-shell structured ZSM-5@t-ZrO_2 catalyst. *Chem. Eng. Sci.* **2019**, *211*, No. 115273.
(46) Huang, F.; Cao, J.; Wang, L.; Wang, X.; Liu, F. Enhanced catalytic behavior for methanol to lower olefins over SAPO-34 composited with ZrO_2. *Chem. Eng. J.* **2020**, *380*, No. 122626.
(47) Zeng, L.; Wang, Y.; Mou, J.; Liu, F.; Yang, C.; Zhao, T.; Wang, X.; Cao, J. Promoted catalytic behavior over γ-Al_2O_3 composited with ZSM-5 for crude methanol conversion to dimethyl ether. *Int. J. Hydrogen Energy* **2020**, *45*, 16500−16508.

https://doi.org/10.1021/acsomega.1c02369
ACS Omega 2021, 6, 19067−19075